Xiang, J., Du, J., Li, D., & Scarpa, F. (2017). Numerical analysis of the impact resistance in aluminium alloy bi-tubular thin-walled structures designs inspired by beetle elytra. *Journal of Materials Science*, *52*(22), 13247–13260. https://doi.org/10.1007/s10853-017-1420-z

Numerical analysis of the impact resistance in aluminium alloy bi-tubular thin-walled structures designs inspired by beetle elytra

Jinwu Xiang[a], Jianxun Du[a]*, Daochun Li[a], Fabrizio Scarpa[b]

[a]School of Aeronautic Science and Engineering, Beihang University

Beijing, 100191, China.

[b]Advanced Composites Center for Innovation and Science, University of Bristol, Bristol BS8 1TR, UK

Abstract

Thin-walled tubular structures are commonly used in automotive and aerospace applications because of their high strength and lightweight characteristics. In this paper we propose a new bionic bi-tubular thin-walled structure (BBTS) inspired from the internal structure of the lady beetle elytron. Six types of BBTSs with different geometric parameters and same type of material were simulated under axial dynamic impact loading with a weight of 500 kg and a velocity of 10 m/s using nonlinear finite elements. The comparison between BBTSs with equal mass shows that the thickness of the inner wall and the cross-sectional configurations influence significantly the energy absorption of the structure. BBTSs show an optimized crashworthiness behavior when the inner wall thickness is between 1.6 mm and 2.0 mm. In addition, circular and octangular BBTSs show improved absorption characteristics when the inner wall thickness is 2.0 mm. We also evaluate the energy absorption of periodically distributed BBTS against cellular configuration with irregular topology. The energy absorption characteristic of BBTS with regular distribution is better than that of BBTS with irregular distribution, which indicates that the optimized regular structure has an improved mechanical performance to the original bionic topology.

Keywords: electron microscopy; finite element method; aluminium alloys; honeycomb structure

Corresponding author: Jianxun Du

Corresponding author's institution: Beihang University

E-mail: dujianxun@buaa.edu.cn

1. Introduction

Thin-walled tubes with a simple cross-section shape are commonly used as energy absorbers because they are relatively easy to manufacture and efficient in terms of energy absorption. During the past decade the behavior under axial impact of thin-walled tubes with different materials and structures has been investigated using combinations of theoretical analysis [1], numerical simulations [2,3]and experimental tests [3,4,5]. Different cross-sectional shapes of single thin-walled tube significantly affect the efficiency of the energy absorption process. Four simple geometries such as hexagon, octagon, 12-sided, and 16-sided star have been already evaluated from an experimental point of view[6], and the results have shown that an increase in the number of inward corners tends to improve the energy absorption capabilities. Other geometries have also been extensively studied, such as circular[7,8], square[9,10], rectangular[11,12,13], hexagonal[14,15,16], pyramidal[17]and conical tubes[18,19,20]. More recently two novel geometries with different materials (pentagon and cross-type section) have been also investigated [21]. A configuration that combines the square and circular sections has also been proposed and the simulation results have shown that the crashworthiness performance of this new structure is improved compared to the analogous performance from the single square or circular sections[22].The temperature has also been shown to have a significant effect on the material behavior and the crashworthiness of steel-plated structures in terms of brittle fracture and mean crushing loads [23]. A new design solution [24]has also been proposed to improve the energy absorption efficiency of a thin-walled column by introducing extra stable corners in the cross-section. Some authors have conducted parametric studies[25,26,27,28]on longitudinally grooved square tubes under axial crushing. From those simulation results, it is apparent that the introduction of grooves significantly increases the specific energy absorption of the columns. Some experimental studies[29,30] of the thin-walled tubes with patterned windows have also been carried out, together with the numerical analysis of the three collapse modes characteristics. and changes in length and thickness of the tube segments to control the crush force [31].

Bi-tubular thin-walled column designs are also reported in open literature. From a general point of view, bi-tubular configurations have improved energy absorption characteristics compared to the single thin-walled tube case. Several complex geometric parameters of bi-tubular

configurations have been numerically investigated, including the radial distance of concentric cylindrical tubes[32], the shape and the size of the inner tubes, and the location of the diaphragms[33]. Other research papers[7,34,35]have dealt with foam-filled bi-tubular circular tubes subjected to compression loading, and related parameter conditions like the geometry and the loading type. A novel bi-tubular structure filled with a honeycomb structure with a polygonal configuration has also been investigated numerically. The results have shown that this configuration had favorable energy absorption characteristics in various loading situations compared with the single thin-walled column case [36].

Although a considerable body of research exists on thin-walled structures, it is still an academic and technological challenge to make the tubular configuration more effective in terms of load bearing characteristics, and also easier to manufacture. Animals in nature tend to feature excellent topological and mechanical designs that evolved over eons under challenging environmental conditions[37]. Bionic structural configurations have been employed to design thin-walled tubes[38,39,40,41], but only few research papers have focused on the mechanical properties of the bionic tubular design that bio-mimics the internal structure of the lady beetle elytron [42]. This paper presents a novel bionic bi-tubular thin-walled structure (BBTS) similar to the one observed in the ladybeetle elytron. The energy absorption characteristics of the BBTS with different cross-sectional shapes have been investigated from a numerical standpoint. A parametric analysis of the impact compressive behavior of the structures versus different diameters of the inside tube has also been performed.

2. Ladybeetle-based BBTS

2.1 Structural crashworthiness criteria

Four indicators are used to define the crashworthiness performance of the BBTS[43]. The first indicator to estimate the energy absorption capabilities of the structure is the specific energy absorption (SEA) defined as the ratio of the total energy EA absorbed by a structure to its mass M:

$$\mathrm{SEA} = \frac{\mathrm{EA}}{\mathrm{M}} \tag{1}$$

The area under the force-displacement curve represents the amount of absorbed energy EA:

$$EA = \int_0^d F\ (x)\ dx \tag{2}$$

Where d is the axial crushing displacement and F denotes the axial crushing force. For an energy absorption structure, a high value of crash load efficiency (CLE) is expected:

$$CLE = \frac{MCF}{MIF} \times 100\% \tag{3}$$

Where MIF represents the peak force in the force versus displacement curve under the axial impact. The mean crush force (MCF) for a given deformation can be obtained as:

$$MCF = \frac{EA}{d} \tag{4}$$

2.2 The internal structure of the ladybeetle's elytron

It is well known that the lady beetle elytron protects its flexible wing and body from damage. Lomakin et al. have found that the beetle elytron of Tenebrio is ductile and soft with a Young's modulus (E) of 44±8 MPa, but it becomes brittle and stiff with an E of 2400±1100 MPa when fully tanned. With increasing tanning, dynamic elastic moduli (E') increase nearly 20-fold, whereas the frequency dependence of E' diminishes.[44] Fig. 1 shows a species of ladybeetle, *Coccinella septempunctata*, which is the most common ladybeetle in Europe. Its elytra are red with seven black spots [45]. Fig. 1 also shows the internal microstructure of the elytron of the ladybeetle by optical microscope. It is possible to observe the presence of small independent honeycomb structures with multiple shapes including triangular, rectangular, hexagonal, and circular. Remarkably, it is possible to note the existence of a hollow cylindrical column in the center of all these independent thin-walled structures, as shown in Fig. 2. Fig. 2a shows the presence of a cylindrical column, and the cylindrical tube is also represented by a thin-walled structure (Fig.2b). In nature, the elytron of the lady beetle can resist to an impact load represented by droplets of rain, or produced by an opponent. It is therefore possible to imagine that the bionic bi-tubular thin-walled structures may possess excellent energy absorption characteristics when subjected to impact loading.

2.3 Schematic model for the elytron internal structure

From the observations of the forewing internal structure it is possible to evince that the

elytron of the lady beetle can be schematically represented as a sandwich structure, although the specific elytron microstructure is quite complex. The sandwich representative model is shown in Fig. 3. The upper and lower skins are composed by chitin fibers, and they separate small honeycombs units with different shapes. Nested in each honeycomb unit one can find a hollow column with a circular cross-section. The presence of honeycomb cells with the hollow columns enhance the bending and compressive strength of the forewing structure and reduces the elytron weight to make the flight of the lady beetle easier.

2.4 The design of BBTSs

In this study we have developed six different types of BBTS cross-section inspired to the honeycomb cells of the elytron. The shapes of the BBTSs include triangles, quadrangles, pentagons, hexagons, octagons and circles(Fig. 4). To investigate the energy absorption performance of the different shapes, BBTS samples with equivalent total cross-sectional areas and identical length have been developed. As shown in Table 2, the inner diameter d and the thickness t of inner wall of the BBTSs was chosen as the design variables. The width H of the cross-section in different outer walls was fixed, as well as the thickness of all the outer walls of the cross-sections (2mm).

2.5 Mechanical properties of the base material for the BBTSs

The single-wall tubes were prepared using aluminum alloy AA6063 T6. The specific alloy has a density ρ=2.7×10^3 kg/m^3, a Young's modulus E=68.2 GPa, the initial yield stress σ_y=162MPa, the ultimate stress σ_u=192 MPa, and Poisson's ratio υ=0.3 (see Table 1)[46]. The tubes were modeled with the MAT_24 material law in LS-DYNA971.This aluminium alloy exhibits small strain rate sensitivity, the static stress-strain relationship is presented in Fig.5.[47] The fracture behaviour of the aluminum alloy was neglected during these analyses.

3 Numerical simulations

3.1 Finite element modeling

A scheme representing the BBTS loading conditions of the finite element model is shown in Fig. 6. The bottom of the tube is clamped to the fixed bottom plate. The impactor and the fixed bottom plate are set as rigid bodies. A 500kg rigid impactor with a constant velocity (v=10m/s) is

used to simulate the axial loading on the tubes. An automatic contact setup is used in the numerical simulation to consider the contact caused by the deformation of the tubular wall during crushing. The point-surface contact algorithm is adopted to consider the contact between the BBTS and the rigid wall. The dynamic and static friction coefficients during contact are set at 0.2 [38]. To avoid a zero energy deformation mode and volumetric locking a stiffness-based hourglass control and a reduced integration are used. The material failure of the aluminum alloy tube is neglected [48].

The commercial software CATIA V5R20 is used to create the solid models representing the BBTSs. Hypermesh 12.0 is used as pre-processor to impart the axial impact conditions, material properties, boundary conditions and meshing. The tube is modeled using the quadrilateral shell element with four nodes, mesh size of about 2.0mm×2.0mm is adopted for the model, the number of meshes is 6800. The constitutive behavior of the thin shell element is based on an elastic–plastic material model with Von Mises isotropic plasticity algorithm with piecewise linear plastic hardening. The solver from the explicit nonlinear finite element software LS-DYNA is employed for the simulations; post-processing is treated using the Hyperview 12.0 and Hypergraph 12.0 softwares.

Fig. 7 shows the curves related to the crushing force versus displacement for the the triangular bi-tubular tube with five different mesh densities. The error provided by the models comprising element sizes of 1.5 ×1.5 mm and 2.0×2.0 mm is quite small, and the two mesh sizes show to provide sufficient accuracy to describe the crushing process. To reduce the computational cost, the mesh size of 2.0 ×2.0 mm has been therefore adopted for all the following studies.

3.2 Validation of the finite element model

Lee et al. [49]have carried out experiments for thin-walled square columns under axial impact loading. In their experiments they adopted aluminum AL6063 thin-walled extruded tubes with lengths of 200 mm. The weight of the cross head was 40 kg, and the impact velocity was 7.02 m/s. These values are chosen to meet the impact energy requirements for vehicles. These chosen values are in effect to provide safety for the car drivers and the passenger seated in the front cabin[50]. To validate our FE models, we have first reproduced the same types of empty single thin-walled square tubes with the same sizes and axial impact loading conditions, and compared

our results with the experimental data of Lee et al. Figs.7 and 8 show the comparisons between the experiments and the simulations. Fig. 8 shows that the collapse mode produced by the numerical simulations matches quite well the one from the experiments. Although the collapse mode of structure is similar enough between experiment and numerical simulation, the shapes of folds are still not very consistent. It may caused by the setting values in numerical computational software are still not very suitable. On the other hand, the experimental parameters and material properties which used for experiment in the literature are still not very accurate and detailed. Moreover, Fig. 9 shows the simulation curve of the crushing force versus displacement agrees well with the one from the experiments. These results validate our FE modeling approach for the subsequent use in evaluating the crushing performance of the BBTSs.

3.3 Numerical simulations of the BBTSs

The energy absorption characteristics of the BBTSs under axial crushing loading appear to be strongly related to their cross-sectional geometry. It is therefore important to analyze the correlation between the structural and geometry parameters of the BBTSs and their mechanical characteristics. We use in this paper crashworthiness metrics such as SEA, MIF, and CLE to compare the numerical predictions with the different parameters defining the bi-tubular structures.

3.3.1 Effect of the outer wall cross-sectional shape

To assess the differences between the six types of outer wall cross-sectional shapes we have carried out numerical simulations on models with the same inside column (t = 0.8 mm) and a different outside tube. The evolution of the BBTS shapes under different axial displacements are shown in Fig. 10 (a-f).The BBTS collapse is strongly affected by the interaction between the inner and outer tubes (Fig. 10(a)). Fig. 10 (f) shows that the outside structure and inside column of each BBTS assume the dynamic deformation during the crushing process. Fig. 11 shows the crushing force versus displacement for all the tested structures. The absorbed energy-displacement curves for the different cross-sections are shown in Fig.12. The two figures show that the crushing force and the absorbed energy of the circular and octagonal BBTSs are slightly higher than the ones pertaining the other BBTSs. The absorption characteristics of the triangular BBTS are enhanced compared to the ones of the rectangular BBTS due to the strong interaction between the internal triangular structures. Because the distance between the inner and outer surfaces of triangular

BBTS is very close, the absorbed energy of the entire triangular BBTS is more than sum of absorbed energy by inner and outer tubes loaded separately. The interaction between the inner and outer tube increase the absorbed energy of the triangular BBTS. So the absorbed energy of triangular BBTS is always bigger than the one of rectangular BBTS, as show in Fig.12. The SEAs, MIFs, and CLEs of the BBTSs are compared in Fig. 13. The SEA and CLE metrics are affected by the changes in the cross-sectional shape, while the CLE of BBTS appeared not to change. According to Fig.13, it can be seen that SEA and CLE of BBTS changed a lot with the change of the structure thickness. However, the MIF presents irregular change when the thickness increased. Among the 6 cases, BBTS with the thickness of 2.0mm has the highest SEA and CLE, and BBTS with the thickness of 1.2mm has the highest MIF. The SEA value gradually increases when the cross-sectional shape changes from triangular to circular (Fig. 13(a)). The BBTS with a octagonal cross-section in the 1.6 mm thickness group has the highest SEA value. Compared with the octagonal BBTS, the SEA value of the BBTS with a circular cross-section is lower. The SEA value of BBTS with circular ones is higher than the corresponding values related to other BBTSs, and this is in agreement with results from open literature[51]. The above results indicate that the increase in SEA and CLF is due to the increase in number of edges. Although the BBTSs with octagonal cross-section with t = 1.6 mm and 2.8 mm show between the highest CLE values, the BBTS with circular cross-section with t = 2.0mm appears to possess the most ideal structure for energy absorption among all cases.

3.3.2 Effect of the inner wall

We have designed six shapes of outer wall cross-section to study the energy absorption characteristics pertaining to different thicknesses of the inner wall under the same outer wall configurations. The six shapes were divided into six groups. In each group the thickness of the inner wall (t=0.8 mm, 1.2 mm, 1.6 mm, 2.0 mm, 2.4 mm, and 2.8 mm) gradually decreases as the diameter of the inner wall increases. This has been done to maintain constant the total area of each inner wall cross-sectional shape. Fig. 14 (a-f) shows the deformations of the hexagonal BBTSs with different inner wall thicknesses. The BBTS with a larger diameter undergo an ideal (i.e., almost uniform) deformation, whereas the BBTS with a smaller diameter (Fig. 14. d-f) show a global buckling deformation on the inner tube. Fig. 15 shows the behavior of the crushing force versus displacement for the BBTSs considered. The absorbed energy versus the crushing

displacements of the different cross-sections is shown in Fig. 16. The two figures demonstrate that the crushing force and absorbed energy of some of the hexagonal BBTSs (t= 1.2 mm, 1.6 mm, and 2.0 mm) are slightly higher than the other similar configurations. Because of the inside tube of some BBTS with t= 2.4 mm and 2.8 mm shows a strong tendency to buckle the absorption characteristic of these two types of BBTS are slightly worse than the BBTSs with t= 1.2 mm, 1.6 mm and 2.0 mm. The SEAs, MIFs, and CLEs calculated for the different inner walls are compared in Fig.17. All three metrics tend to first increase and then decrease as the inner wall thickness assumes higher values. For each shape the highest SEA is in general provided by inner wall thickness of 1.6 mm and 2.0 mm (Fig.17 (a)). When the inner wall thickness is 1.2 mm, the value of the MIF is the highest independently from the particular shape adopted (Fig.17 (b)). Amongst all the cases considered the highest value of the MIF is provided by the inner wall thickness of t=1.2 mm and an octagonal outer wall shape. The CLE values gradually increase when the outer wall cross-sectional shape changes from triangular to circular (Fig. 17(c)). For each shape group the highest values of CLE reside between inner wall thicknesses of 1.6 mm and 2.0 mm. The peak of CLE value observed in our simulations corresponds to the case in which the thickness of the inner wall is 2.0 mm for the circular group.

3.3.3 A comparison between two types of honeycomb BBTSs

Following the single units BBTS simulations, we have performed a numerical experiment to compare the energy absorption performance of regular and irregular BBTS. Honeycombs made from hexagonal, octagonal and circular units show improved better energy absorption capabilities when the cells are tessellated. From a manufacturing perspective, the hexagonal structure is in general preferred, and therefore we have adopted this shape for the regular BBTS honeycombs. Because the hollow tube shows an improved energy absorption capability when the diameter is between 18.13 mm and 23.56 mm. In order to maintain the same mass of two types of BBTSs, a size of 19.56 mm has been selected for the regular BBTS honeycomb case. The irregular BBTS comes from direct observations of the elytron microstructure (Fig. 18 (a)). Fig. 18(b) shows the opposite BBTS with regular hexagonal honeycombs. The mass of the regular is the same with that of irregular BBTS. The above two structures have been compared in terms of energy absorbing capabilities. The FE models of BBTS has been established. The numbers of mesh elements for regular and irregular BBTS models are 214491 and 221321, respectively. The bottom of the

models is clamped to the fixed bottom plate. The impactor and the fixed bottom plate are set as rigid bodies. The 500 kg rigid impactor with a constant velocity (v=10 m/s) is used to simulate the axial loading on the BBTS models. Fig. 19 shows that the absorbed energy of the regular BBTS is higher than the one provided by the irregular BBTS. Because of the same mass, the SEA value of regular BBTS is higher than that of the irregular one.

4 Conclusions

In the present study we propose a new type of energy absorbing structure called bionic bi-tubular thin-walled structure (BBTS). The above structure bio-mimics the structural characteristics of the lady beetle elytra. BBTSs with six different cross-sectional configurations of external tubes and six different diameters of inner tubes have been investigated from a numerical standpoint under axial impact loading using the nonlinear finite element code LS-DYNA. By comparing the regular and irregular honeycomb distributions of BBTSs, we have found that the energy absorption characteristics of regular hexagonal BBTS units is higher than the one exhibited by their irregular distribution counterpart. This feature suggests that the optimized regular BBTS unit structure can provide a superior energy absorption performance compared to the original bionic structure. Overall, this study has shown that BBTSs might be proposed as a useful energy absorbing structure in the aerospace and automobile fields to improve impact resistance. Future investigations into the function of the lady beetle elytra would make the bionic engineering more suitable and effective, which could dramatically improve our research quality of crashworthiness.

Acknowledgments

The authors gratefully acknowledge the support from the National Natural Science Foundation of China under grant Nos. 11402014 and 11572023. The authors also acknowledge the financial support from China Scholarship Council.

Conflict of Interest

The authors declare that they have no conflict of interest.

References:

[1] NIKNEJAD, A., JAVAN, Y. T., Circular metal tubes during lateral compression between a V-shape indenter and a platen - Theory and experiment, *Proceedings of the Institution of Mechanical Engineers, Part L: Journal of Materials: Design and Applications* **229**,2015,pp.318-331.

[2] SMITH, D., GRACIANO, C., MARTÍNEZ, G., Axial crushing of flattened expanded metal tubes, *Thin-Walled Structures* **85**,2014,pp.42-49.

[3] ROUZEGAR, J., ASSAEE, H., NIKNEJAD, A., Geometrical discontinuities effects on lateral crushing and energy absorption of tubular structures, *Materials & Design* **65**,2015,pp.343-359.

[4] SMITH, D., GRACIANO, C., MARTÍNEZ, G., Quasi-static axial compression of concentric

expanded metal tubes, *Thin-Walled Structures* **84**,2014,pp.170-176.

[5] NIKNEJAD, A., REZAEI, B., LIAGHAT, G. H., Empty circular metal tubes in the splitting process – theoretical and experimental studies, *Thin-Walled Structures* **72**,2013,pp.48-60.

[6] FAN, Z., LU, G., LIU, K., Quasi-static axial compression of thin-walled tubes with different cross-sectional shapes, *Engineering Structures* **55**,2013,pp.80-89.

[7] AZARAKHSH, S., RAHI, A., GHAMARIAN, A., Axial crushing analysis of empty and foam-filled brass bitubular cylinder tubes, *Thin-Walled Structures* **95**,2015,pp.60-72.

[8] CHIU, L. N. S., FALZON, B. G., RUAN, D., Crush responses of composite cylinder under quasi-static and dynamic loading, *Composite Structures* **131**,2015,pp.90-98.

[9] ZHANG, X., WEN, Z., ZHANG, H., Axial crushing and optimal design of square tubes with graded thickness, *Thin-Walled Structures* **84**,2014,pp.263-274.

[10] NIKNEJAD, A., ABEDI, M. M., LIAGHAT, G. H., Absorbed energy by foam-filled quadrangle tubes during the crushing process by considering the interaction effects, *Archives of Civil and Mechanical Engineering* **15**,2015,pp.376-391.

[11] SHARIATPANAHI, M., MASOUMI, A., ATAEI, A., Optimum design of partially tapered rectangular thin-walled tubes in axial crushing, *Proceedings of the Institution of Mechanical Engineers, Part B: Journal of Engineering Manufacture* **222**,2008,pp.285-291.

[12] NIKNEJAD, A., ELAHI, S. M., ELAHI, S. A., Theoretical and experimental study on the flattening deformation of the rectangular brazen and aluminum columns, *Archives of Civil and Mechanical Engineering* **13**,2013,pp.449-464.

[13] MAHDI ABEDI, M., NIKNEJAD, A., HOSSEIN LIAGHAT, G., Theoretical and experimental study on empty and foam-filled columns with square and rectangular cross section under axial compression, *International Journal of Mechanical Sciences* **65**,2012,pp.134-146.

[14] ZHANG, X., ZHANG, H., Experimental and numerical investigation on crush resistance of polygonal columns and angle elements, *Thin-Walled Structures* **57**,2012,pp.25-36.

[15] AKTAY, L., KRÖPLIN, B. H., TOKSOY, A. K., Finite element and coupled finite element/smooth particle hydrodynamics modeling of the quasi-static crushing of empty and foam-filled single, bitubular and constraint hexagonal- and square-packed aluminum tubes, *Materials & Design* **29**,2008,pp.952-962.

[16] ZAREI MAHMOUDABADI, M., SADIGHI, M., A study on the static and dynamic loading of the foam filled metal hexagonal honeycomb – Theoretical and experimental, *Materials Science and Engineering: A* **530**,2011,pp.333-343.

[17] ALAVI NIA, A., HADDAD HAMEDANI, J., Comparative analysis of energy absorption and deformations of thin walled tubes with various section geometries, *Thin-Walled Structures* **48**,2010,pp.946-954.

[18] MEHMET A. GULER, M. E. C. B., The effect of geometrical parameters on the energy absorption characteristics of thin-walled structures under axial impact loading, *International Journal of Crashworthiness* **15**,2010,pp.377-390.

[19] GHAMARIAN, A., ZAREI, H. R., FARSI, M. A., Experimental and Numerical Crashworthiness Investigation of the Empty and Foam-Filled Conical Tube with Shallow Spherical Caps, *Strain* **49**,2013,pp.199-211.

[20] KATHIRESAN, M., MANISEKAR, K., MANIKANDAN, V., Performance analysis of fibre metal laminated thin conical frusta under axial compression, *Composite Structures* **94**,2012,pp.3510-3519.

[21] ALI, M., OHIOMA, E., KRAFT, F., Theoretical, numerical, and experimental study of dynamic axial crushing of thin walled pentagon and cross-shape tubes, *Thin-Walled Structures* **94**,2015,pp.253-272.

[22] GAO, G., DONG, H., TIAN, H., Collision performance of square tubes with diaphragms, *Thin-Walled Structures* **80**,2014,pp.167-177.

[23] DAE KYEOM PARK, D. K. K. C., On the Crashworthiness of Steel-Plated Structures in an Arctic Environment: An Experimental and Numerical Study, *Journal of Offshore Mechanics and Arctic Engineering* **137**,2015,pp.

[24] REDDY, S., ABBASI, M., FARD, M., Multi-cornered thin-walled sheet metal members for enhanced crashworthiness and occupant protection, *Thin-Walled Structures* **94**,2015,pp.56-66.

[25] DARVIZEH, A., DARVIZEH, M., ANSARI, R., Analytical and experimental investigations into the controlled energy absorption characteristics of thick-walled tubes with circumferential grooves, *Journal of Mechanical Science and Technology* **28**,2014,pp.4199-4212.

[26] DARVIZEH, A., DARVIZEH, M., ANSARI, R., Effect of low density, low strength polyurethane foam on the energy absorption characteristics of circumferentially grooved thick-walled circular tubes, *Thin-Walled Structures* **71**,2013,pp.81-90.

[27] SALEHGHAFFARI, S., TAJDARI, M., PANAHI, M., Attempts to improve energy absorption characteristics of circular metal tubes subjected to axial loading, *Thin-Walled Structures* **48**,2010,pp.379-390.

[28] ZHANG, X., HUH, H., Energy absorption of longitudinally grooved square tubes under axial compression, *Thin-Walled Structures* **47**,2009,pp.1469-1477.

[29] SONG, J., CHEN, Y., LU, G., Light-weight thin-walled structures with patterned windows under axial crushing, *International Journal of Mechanical Sciences* **66**,2013,pp.239-248.

[30] SONG, J., ZHOU, Y., GUO, F., A relationship between progressive collapse and initial buckling for tubular structures under axial loading, *International Journal of Mechanical Sciences* **75**,2013,pp.200-211.

[31] JANDAGHI SHAHI, V., MARZBANRAD, J., Analytical and experimental studies on quasi-static axial crush behavior of thin-walled tailor-made aluminum tubes, *Thin-Walled Structures* **60**,2012,pp.24-37.

[32] ALAVI NIA, A., KHODABAKHSH, H., The effect of radial distance of concentric thin-walled tubes on their energy absorption capability under axial dynamic and quasi-static loading, *Thin-Walled Structures* **93**,2015,pp.188-197.

[33] DONG, H., GAO, G., XIE, S., Collision performance of bitubular tubes with diaphragms, *Journal of Central South University* **22**,2015,pp.3657-3665.

[34] ZHENG, G., WU, S., SUN, G., Crushing analysis of foam-filled single and bitubal polygonal thin-walled tubes, *International Journal of Mechanical Sciences* **87**,2014,pp.226-240.

[35] LI, Z., YU, J., GUO, L., Deformation and energy absorption of aluminum foam-filled tubes subjected to oblique loading, *International Journal of Mechanical Sciences* **54**,2012,pp.48-56.

[36] YIN, H., WEN, G., HOU, S., Crushing analysis and multiobjective crashworthiness optimization of honeycomb-filled single and bitubular polygonal tubes, *Materials & Design* **32**,2011,pp.4449-4460.

[37] NALEWAY, S. E., PORTER, M. M., MCKITTRICK, J., Structural Design Elements in Biological Materials: Application to Bioinspiration, *Advanced Materials* **27**,2015,pp.5455-5476.

[38] LIU, S., TONG, Z., TANG, Z., Bionic design modification of non-convex multi-corner

thin-walled columns for improving energy absorption through adding bulkheads, *Thin-Walled Structures* **88**,2015,pp.70-81.

[39] YIN, H., XIAO, Y., WEN, G., Crushing analysis and multi-objective optimization design for bionic thin-walled structure, *Materials & Design* **87**,2015,pp.825-834.

[40] CHEN, J., XIE, J., ZHU, H., Integrated honeycomb structure of a beetle forewing and its imitation, *Materials Science and Engineering: C* **32**,2012,pp.613-618.

[41] CHEN, J., HE, C., GU, C., Compressive and flexural properties of biomimetic integrated honeycomb plates, *Materials & Design* **64**,2014,pp.214-220.

[42] CHEN, P., LIN, A. Y., MCKITTRICK, J., Structure and mechanical properties of crab exoskeletons, *Acta Biomaterialia* **4**,2008,pp.587-596.

[43] AUDYSHO, R., SMITH, R., ALTENHOF, W., Mechanical assessment and deformation mechanisms of aluminum foam filled stainless steel braided tubes subjected to transverse loading, *Thin-Walled Structures* **79**,2014,pp.95-107.

[44] LOMAKIN, J., HUBER, P. A., EICHLER, C., Mechanical Properties of the Beetle Elytron, a Biological Composite Material, *Biomacromolecules* **12**,2011,pp.321-335.

[45] DOLENSKA, M., NEDVED, O., VESELY, P., What constitutes optical warning signals of ladybirds (Coleoptera: Coccinellidae) towards bird predators: colour, pattern or general look, *Biological Journal of the Linnean Society* **98**,2009,pp.234-242.

[46] YANG, S., QI, C., Multiobjective optimization for empty and foam-filled square columns under oblique impact loading, *International Journal of Impact Engineering* **54**,2013,pp.177-191.

[47] KARAGIOZOVA, D., NURICK, G. N., CHUNG KIM YUEN, S., Energy absorption of aluminium alloy circular and square tubes under an axial explosive load, **43**,2005,pp.956 - 982.

[48] DUARTE, I., VESENJAK, M., KRSTULOVIĆ-OPARA, L., Manufacturing and bending behaviour of in situ foam-filled aluminium alloy tubes, *Materials & Design* **66**,2015,pp.532-544.

[49] LEE, K., YANG, Y., KIM, S., Energy absorption control characteristics of AL thin-walled tubes under impact load, *Acta Mechanica Solida Sinica* **21**,2008,pp.383-388.

[50] REDDY, S., ABBASI, M., FARD, M., Multi-cornered thin-walled sheet metal members for enhanced crashworthiness and occupant protection, *Thin-Walled Structures* **94**,2015,pp.56-66.

[51] YIN, H., WEN, G., HOU, S., Crushing analysis and multiobjective crashworthiness optimization of honeycomb-filled single and bitubular polygonal tubes, *Materials & Design* **32**,2011,pp.4449-4460.

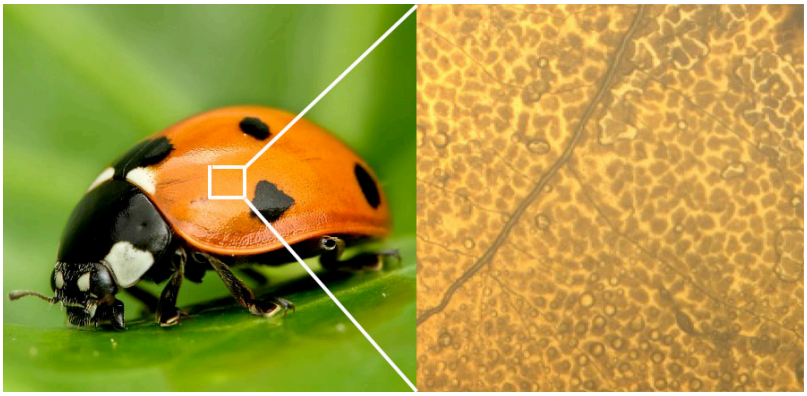

Fig. 1.A Ladybug and the internal structure of its elytron.

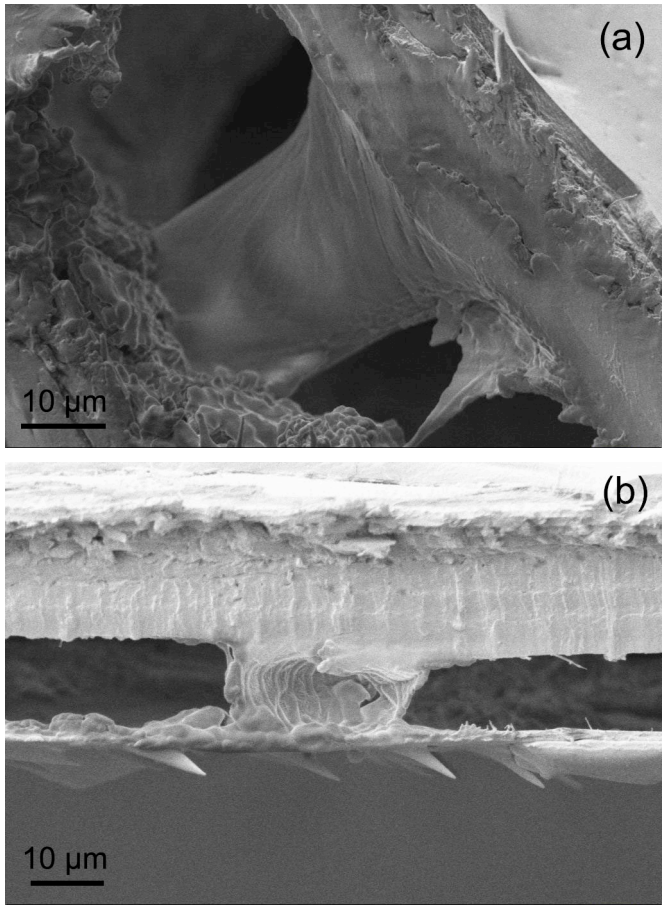

Fig. 2. Microscopic structure of the elytron: (a) the column and (b) the hollow structure of the column.

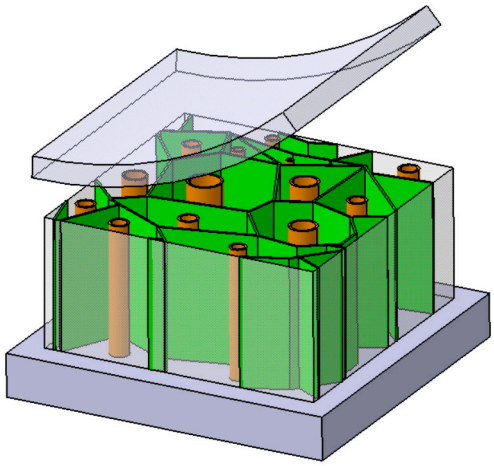

Fig. 3. Schematic view of the honeycomb structure of the elytron.

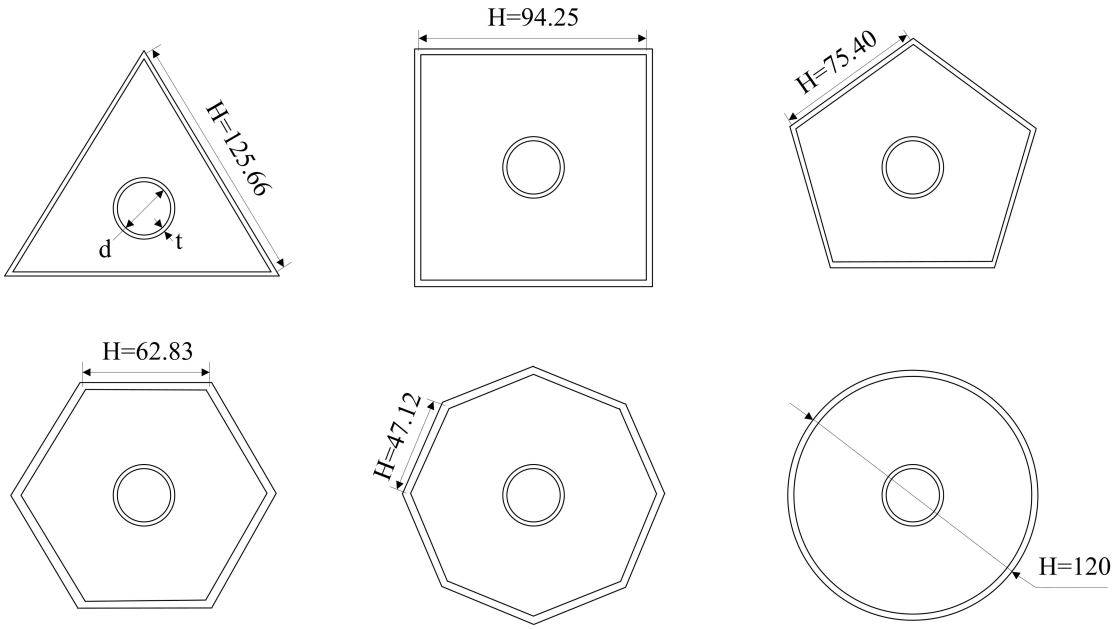

Fig. 4. Cross-section geometry of the BBTSs (all dimensions are in mm)

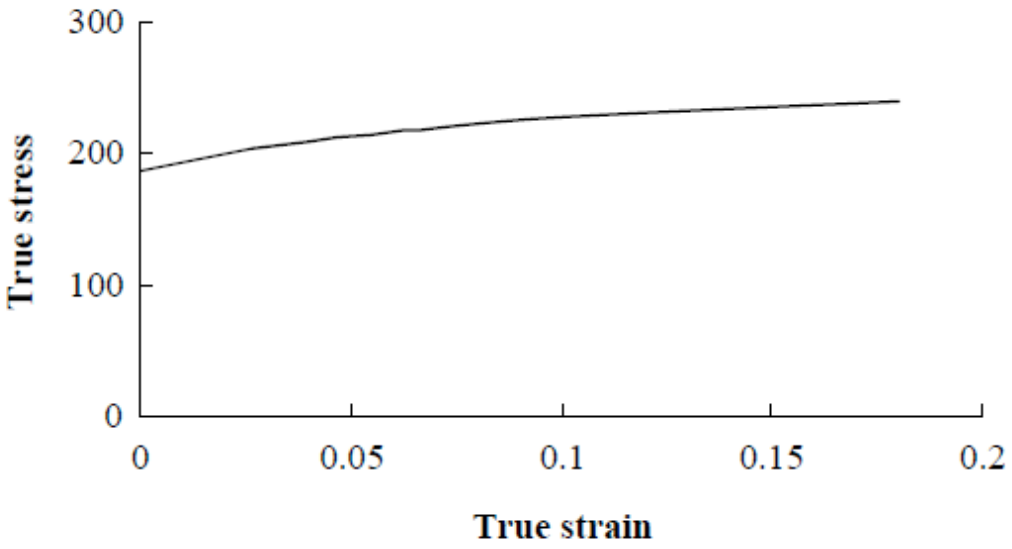

Fig. 5. Static true stress—true strain relationship for Al 6063

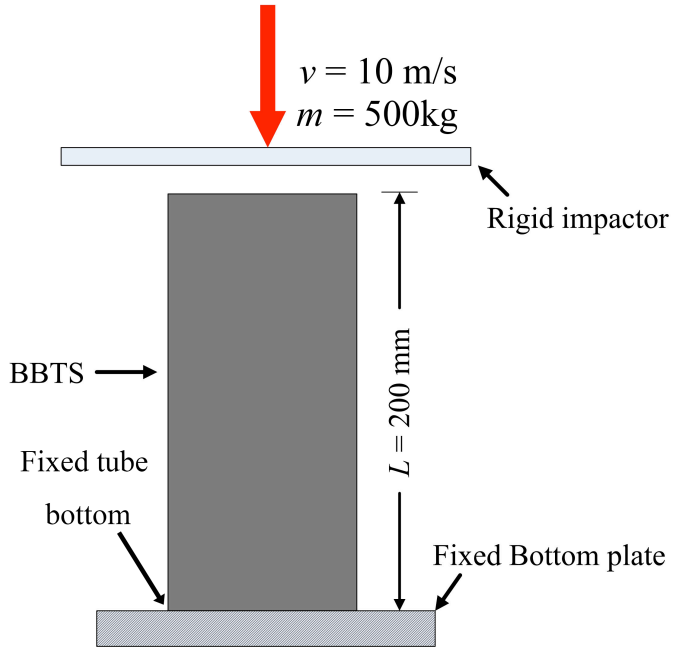

Fig. 6. Schematic of the finite element model subjected to the axial force.

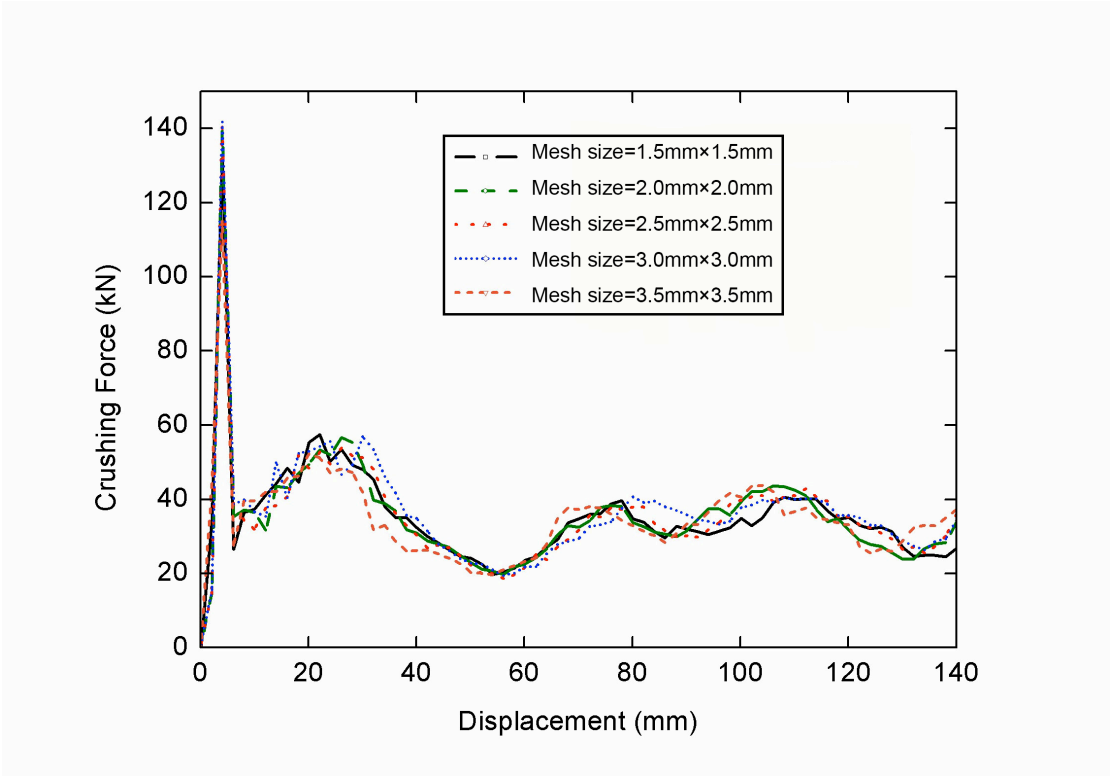

Fig. 7. Crushing forces versus displacements of BBTSs FE models with different mesh sizes.

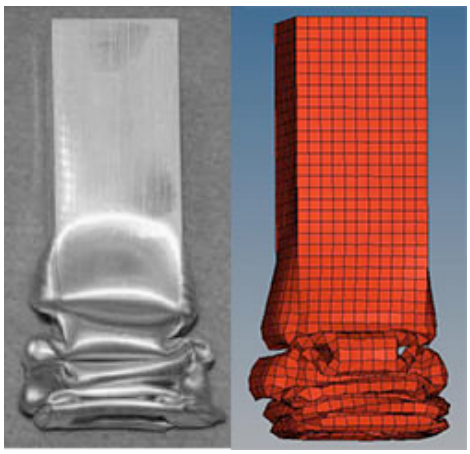

Fig. 8. Comparison between experimental and numerical deformation patterns of a thin-walled structure.

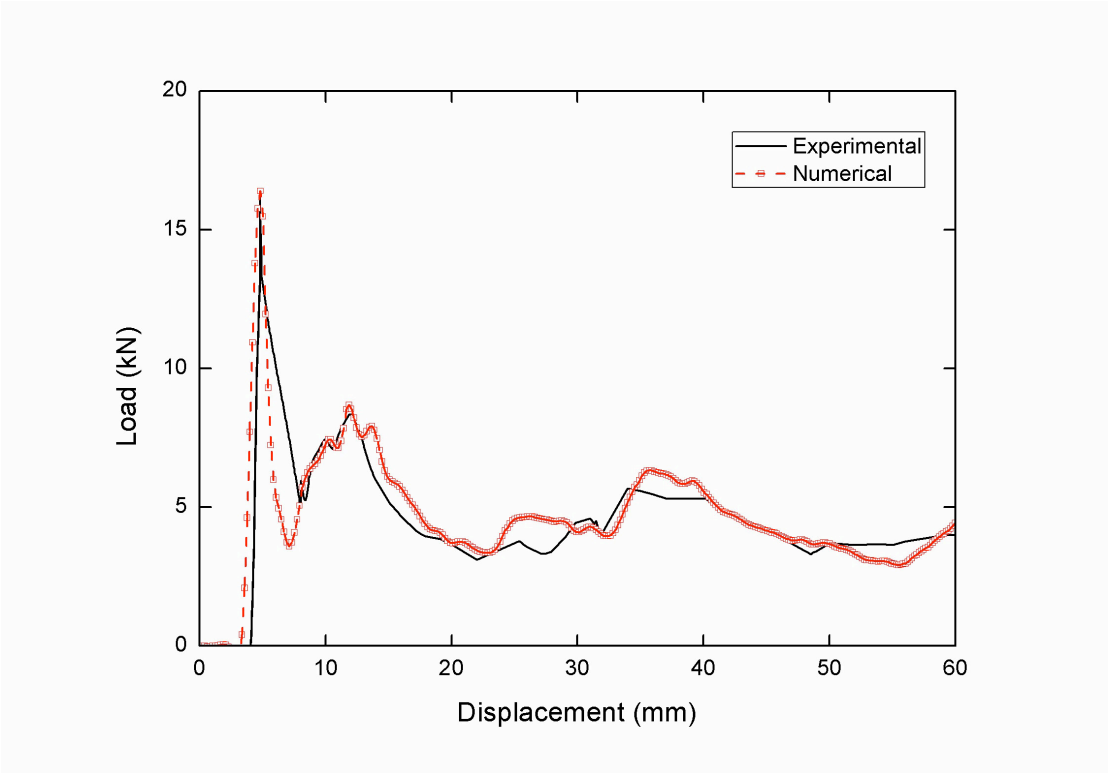

Fig. 9. Comparison of force versus displacement curves between experiment and simulation.

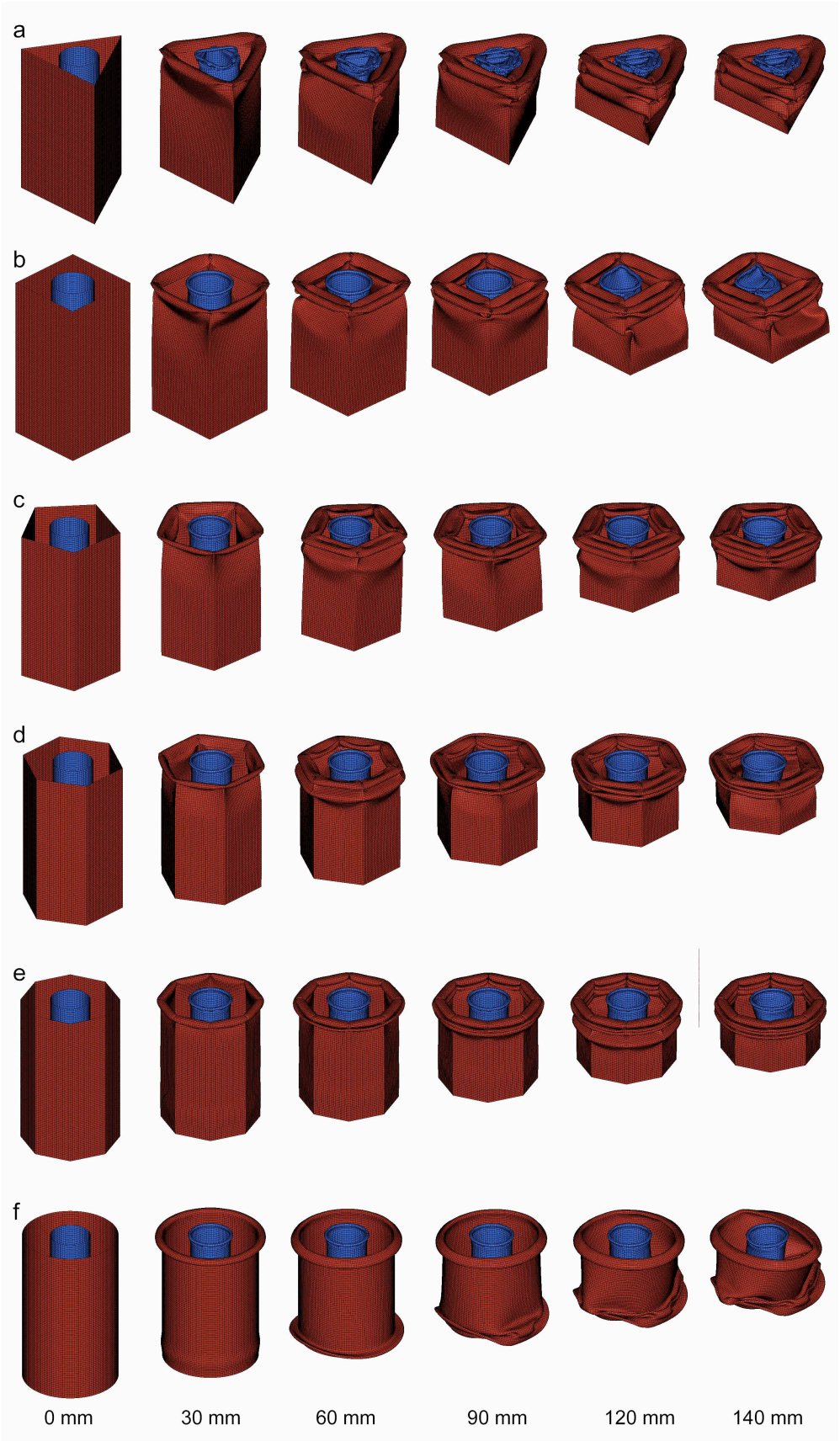

Fig. 10. Progressive collapse of the BBTSs with the same inside column thickness (t= 0.8 mm): (a)triangle,(b) rectangle,(c) pentagon, (d) hexagon,(e) octagon and(f) circular.

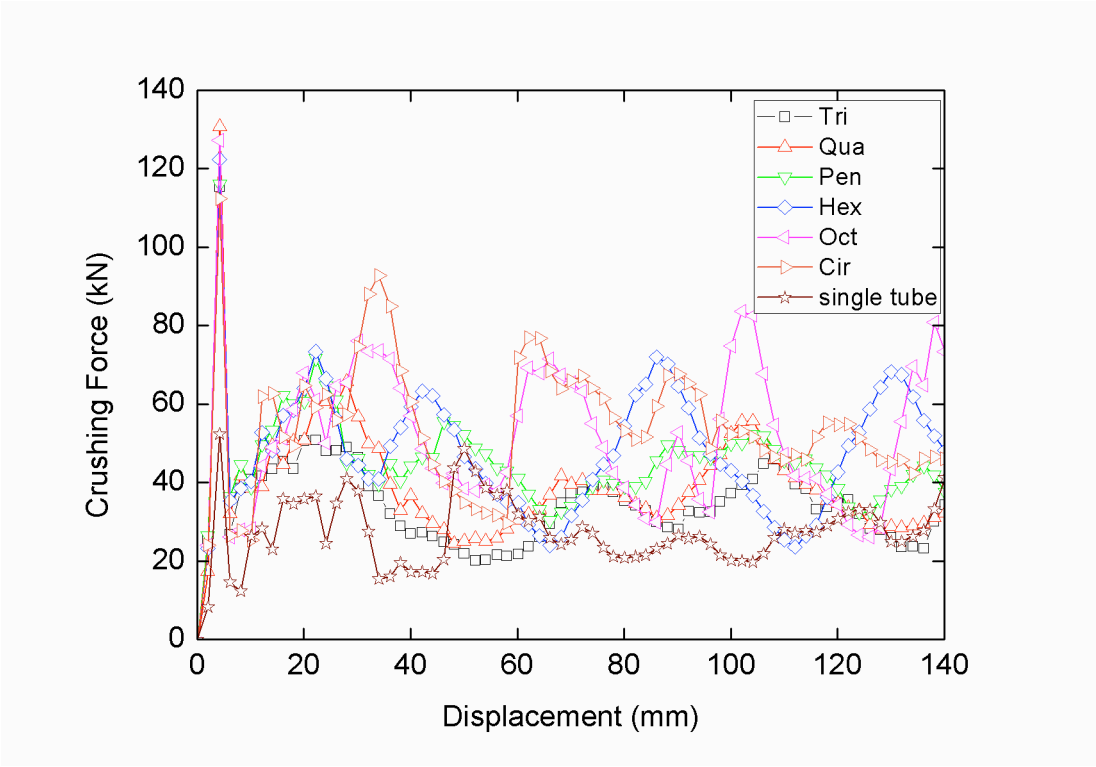

Fig. 11. Crushing force-displacement curves of the outside columns for the different BBTSs shapes (triangle = Tri, rectangle = Qua, pentagon = Pen, hexagon = Hex, octagon = Oct and circular = Cir).

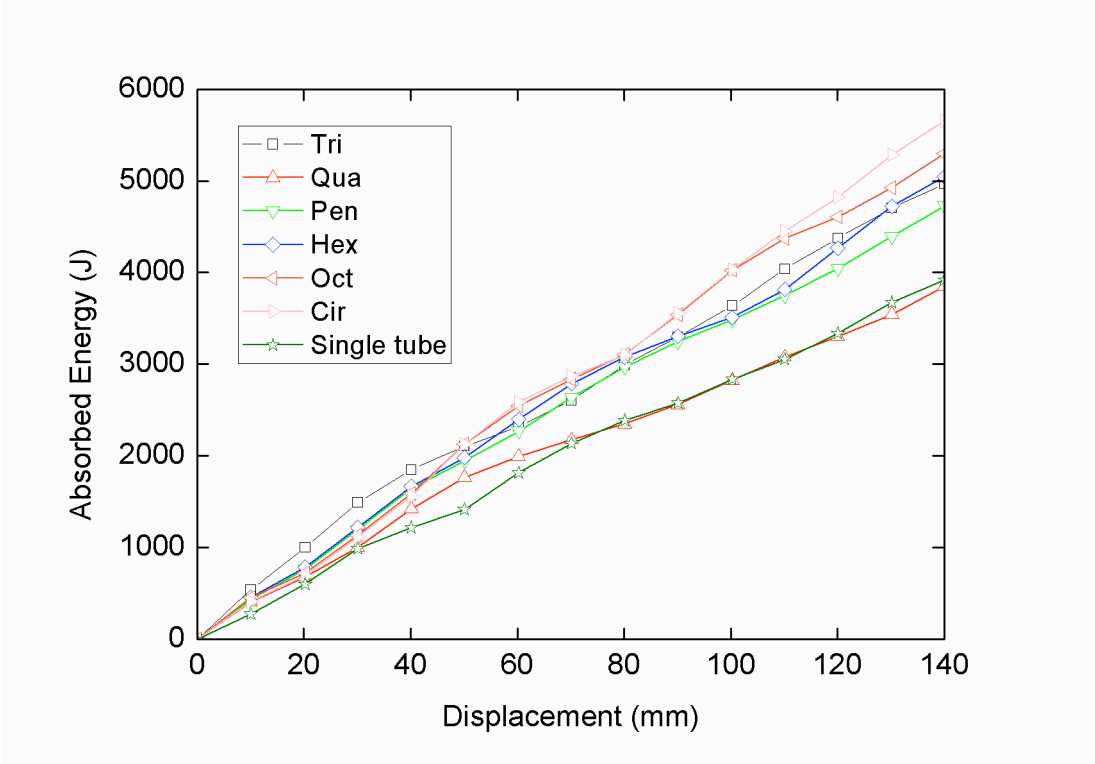

Fig. 12. Absorbed energy- displacement curves of the outside columns for the different BBTSs shapes (triangle = Tri, rectangle = Qua, pentagon = Pen, hexagon = Hex, octagon = Oct and circular = Cir).

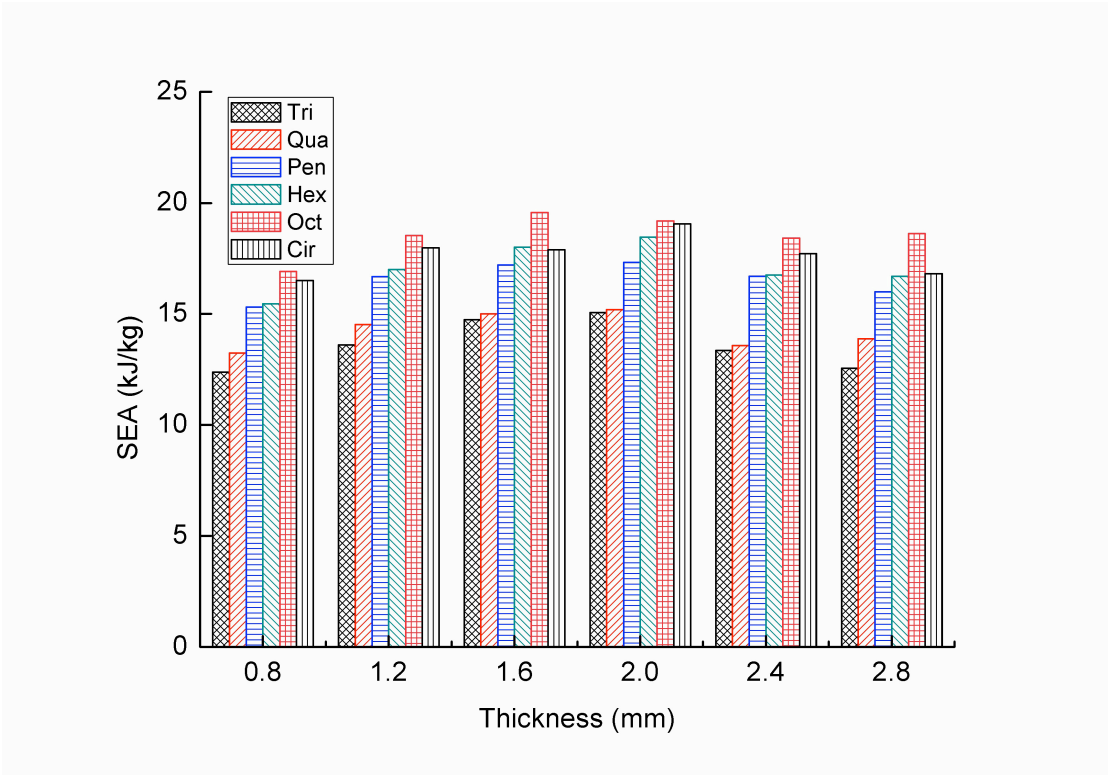
Tri
Qua
Pen
Hex
Oct
Cir
SEA (kJ/kg)
0
5
10
15
20
25
0.8
1.2
1.6
2.0
2.4
2.8
Thickness (mm)

(a)

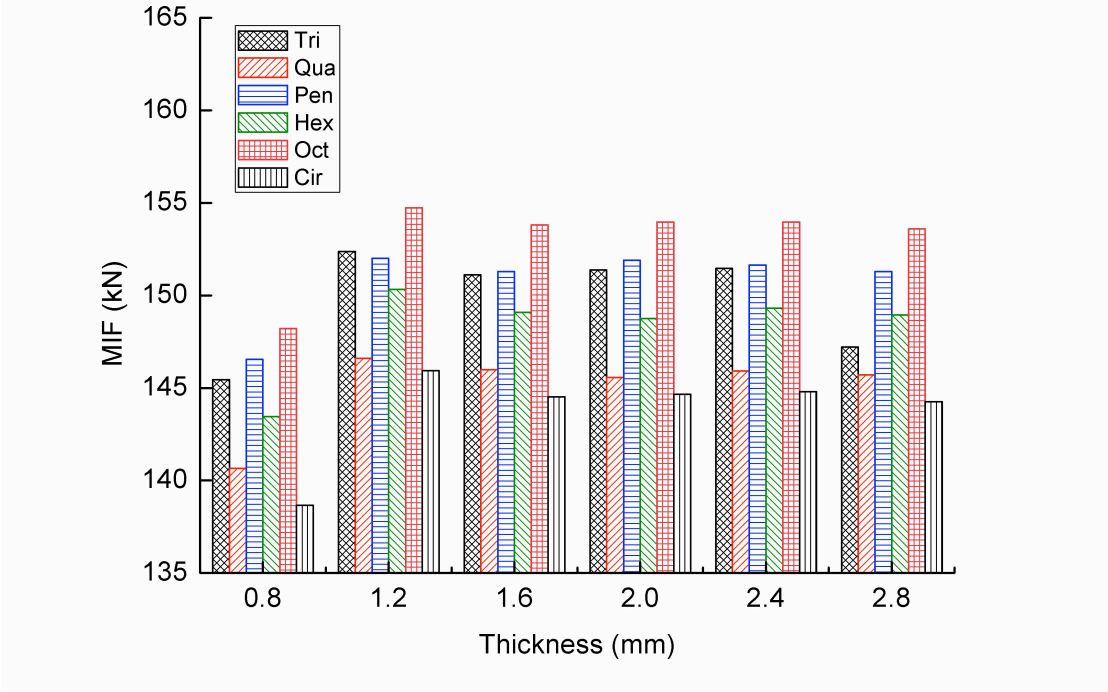
Tri
Qua
Pen
Hex
Oct
Cir
MIF (kN)
135
140
145
150
155
160
165
0.8
1.2
1.6
2.0
2.4
2.8
Thickness (mm)

(b)

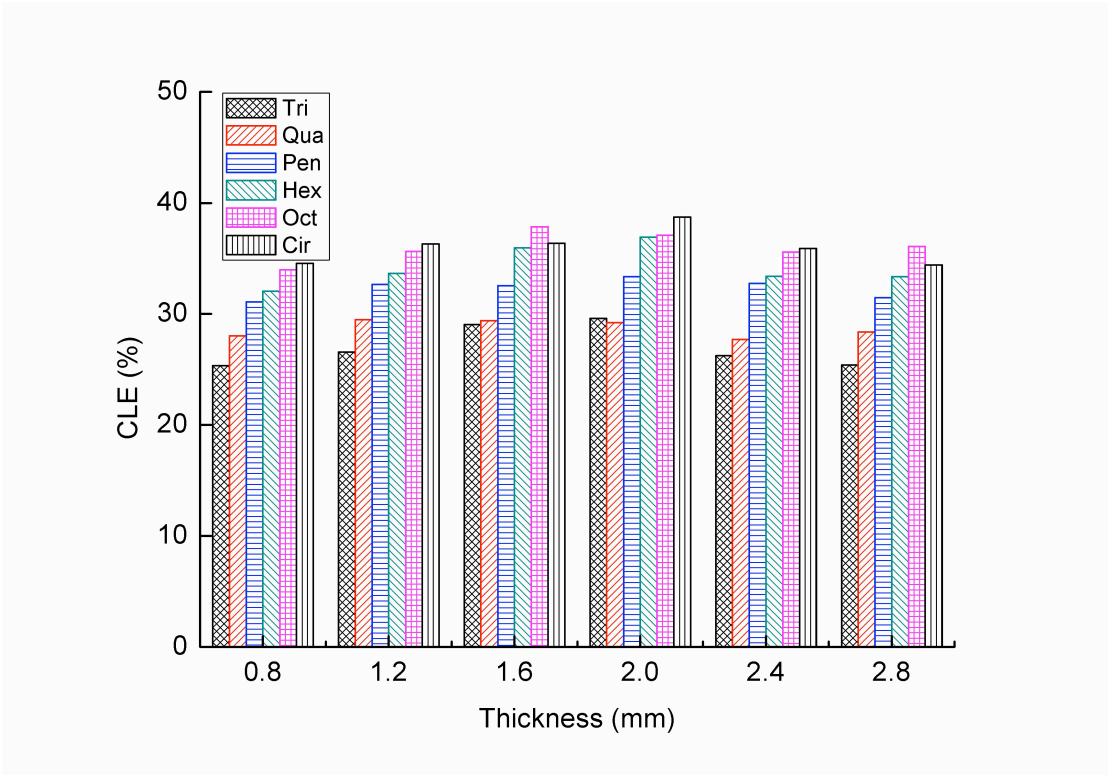

(c)

Fig.13. Crashworthiness metrics of the BBTSs with different cross-section shapes related to the 6 cases: (a) SEAs, (b) MIFs and (c) CLEs.

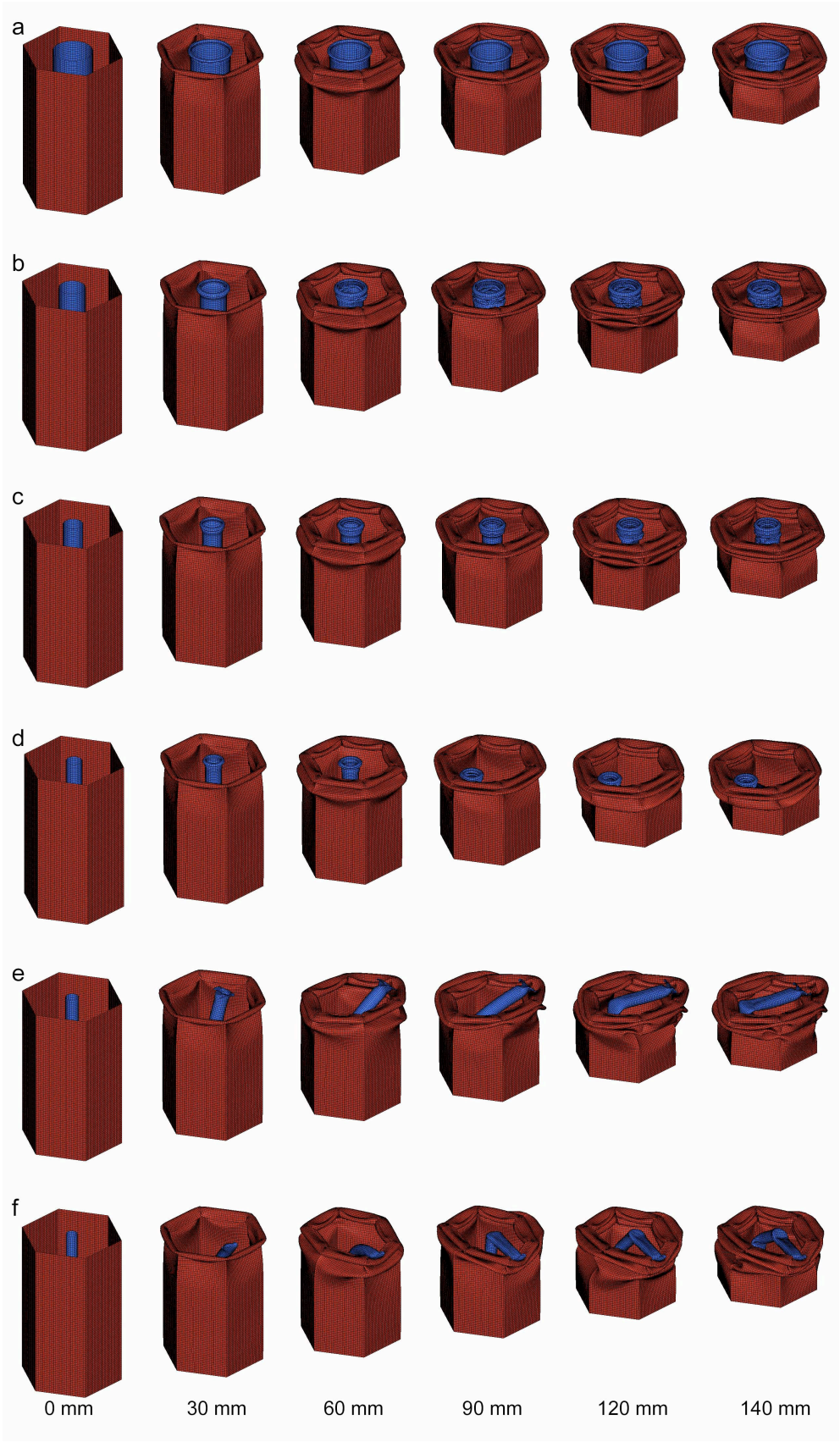

Fig. 14. Progressive collapse of hexagon BBTSs with different inside column thickness: (a)t = 0.8mm, (b) t = 1.2mm, (c) t = 1.6 mm, (d) t = 2.0 mm, (e) t = 2.4 mm and (f) t = 2.8 mm.

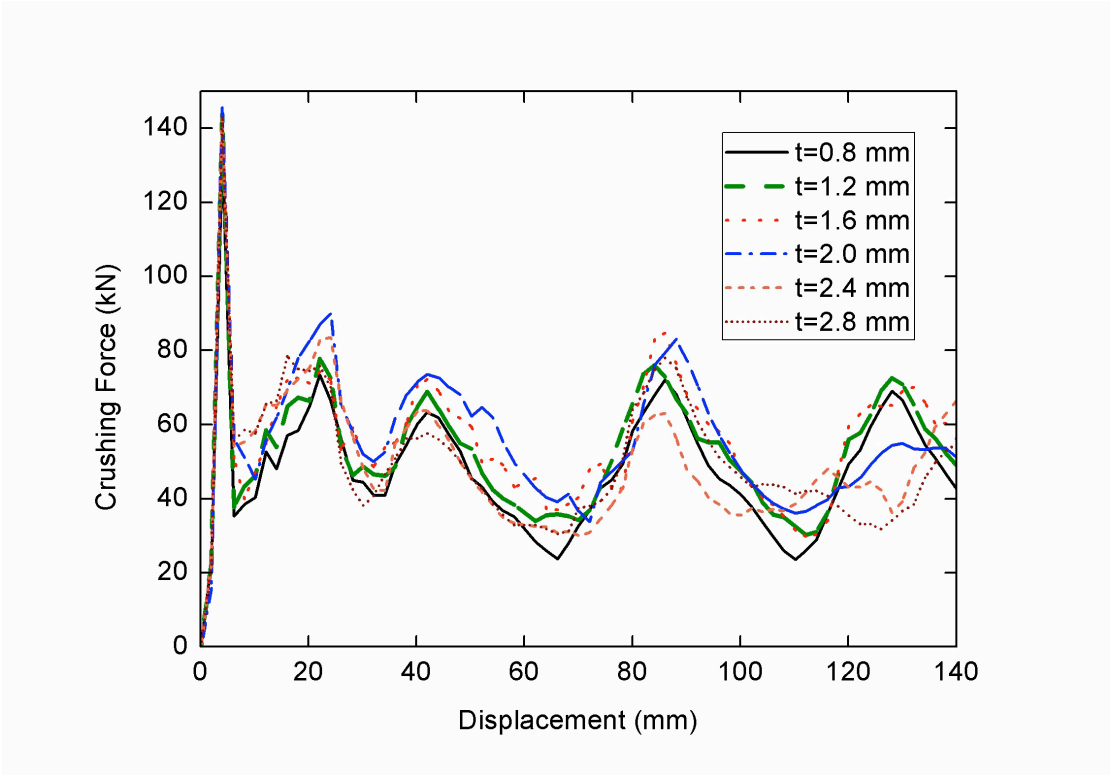

Fig. 15. Crushing force-displacement curves of different thickness of the hexagonal BBTS's inside columns.

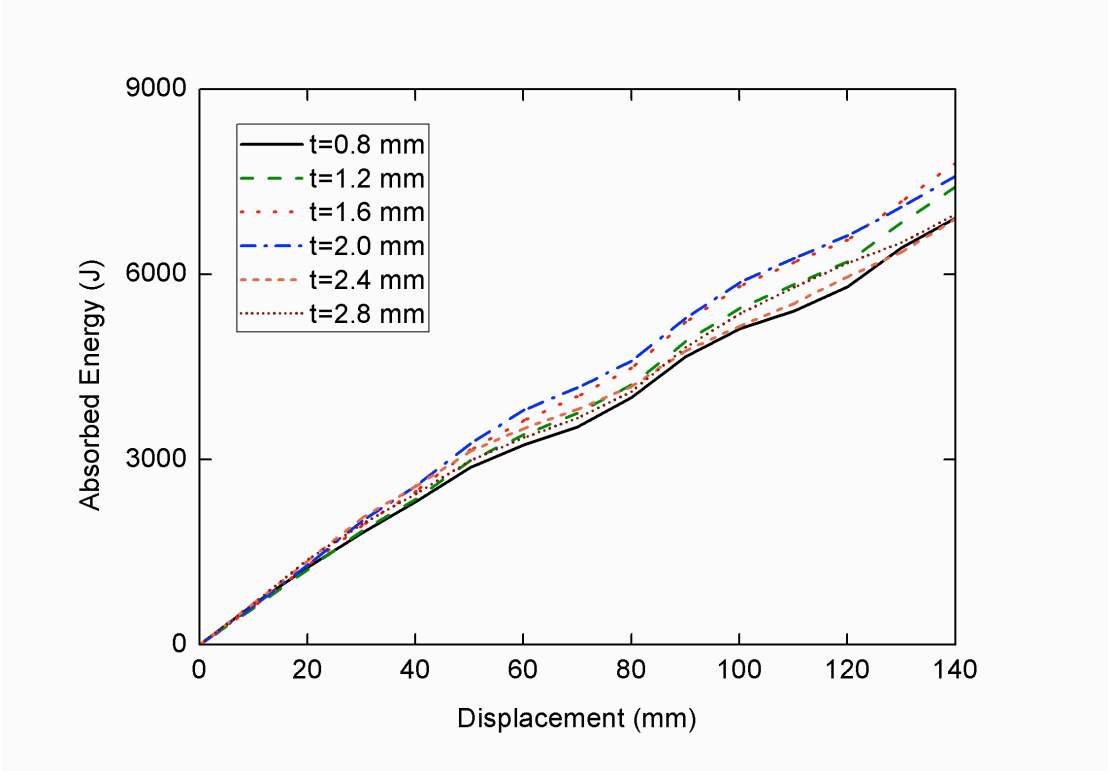

Fig. 16. Absorbed energy versus crushing displacement for the different thickness of the hexagonal BBTSs inside columns.

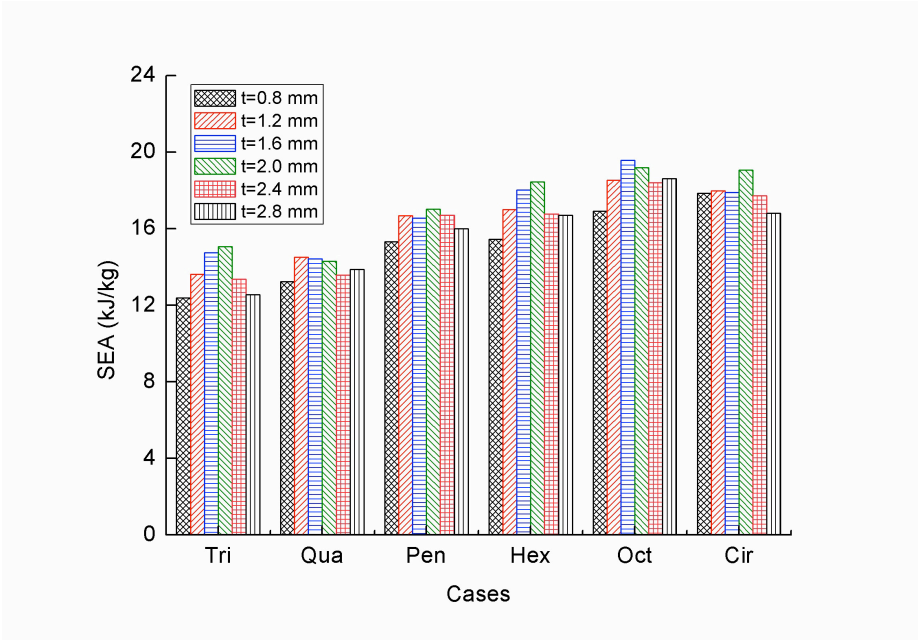
t=0.8 mm
t=1.2 mm
t=1.6 mm
t=2.0 mm
t=2.4 mm
t=2.8 mm
SEA (kJ/kg)
0
4
8
12
16
20
24
Tri
Qua
Pen
Hex
Oct
Cir
Cases

(a)

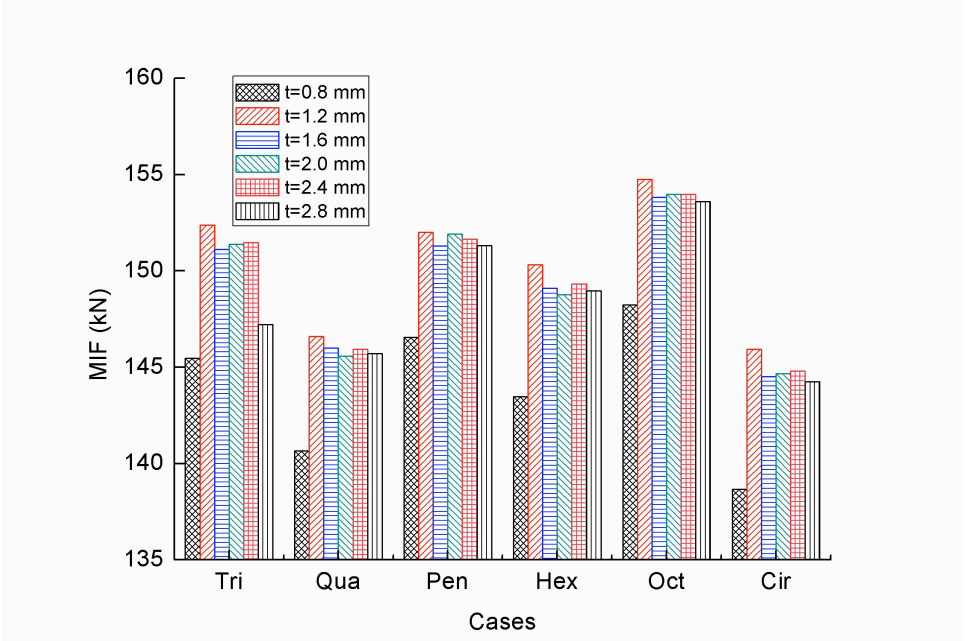
t=0.8 mm
t=1.2 mm
t=1.6 mm
t=2.0 mm
t=2.4 mm
t=2.8 mm
MIF (kN)
135
140
145
150
155
160
Tri
Qua
Pen
Hex
Oct
Cir
Cases

(b)

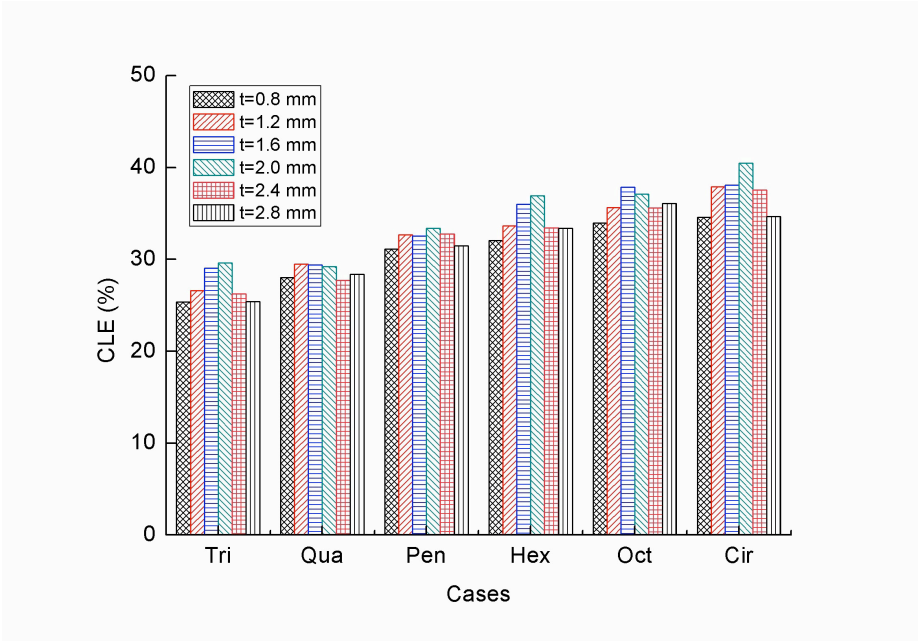

(c)

Fig.17. Crashworthiness metrics for the BBTSs with different inside column diameters for the 6 cases: (a) SEAs, (b) MIFs and (c) CLEs.

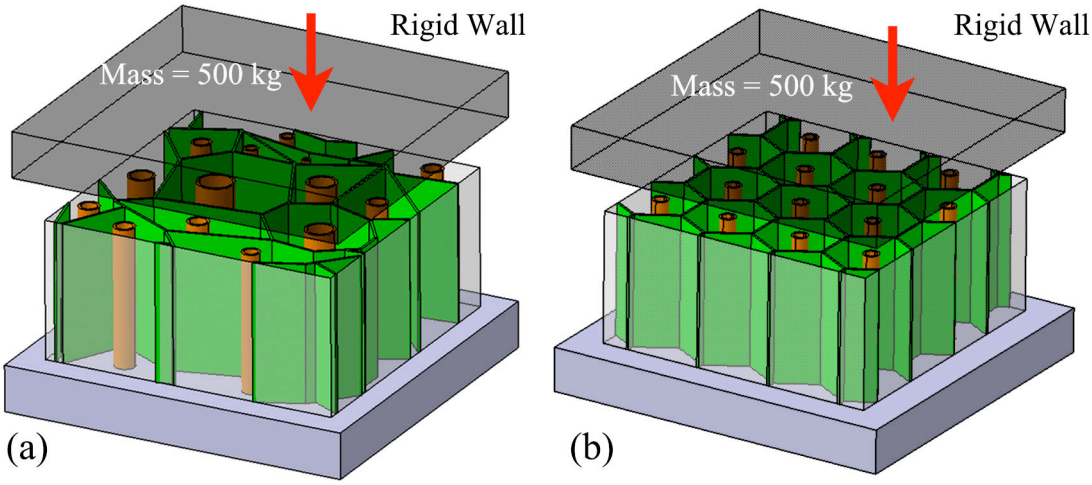

Fig.18. Boundary and initial conditions of FE models of BBTS: (a) irregular BBTS and (b) regular BBTS.

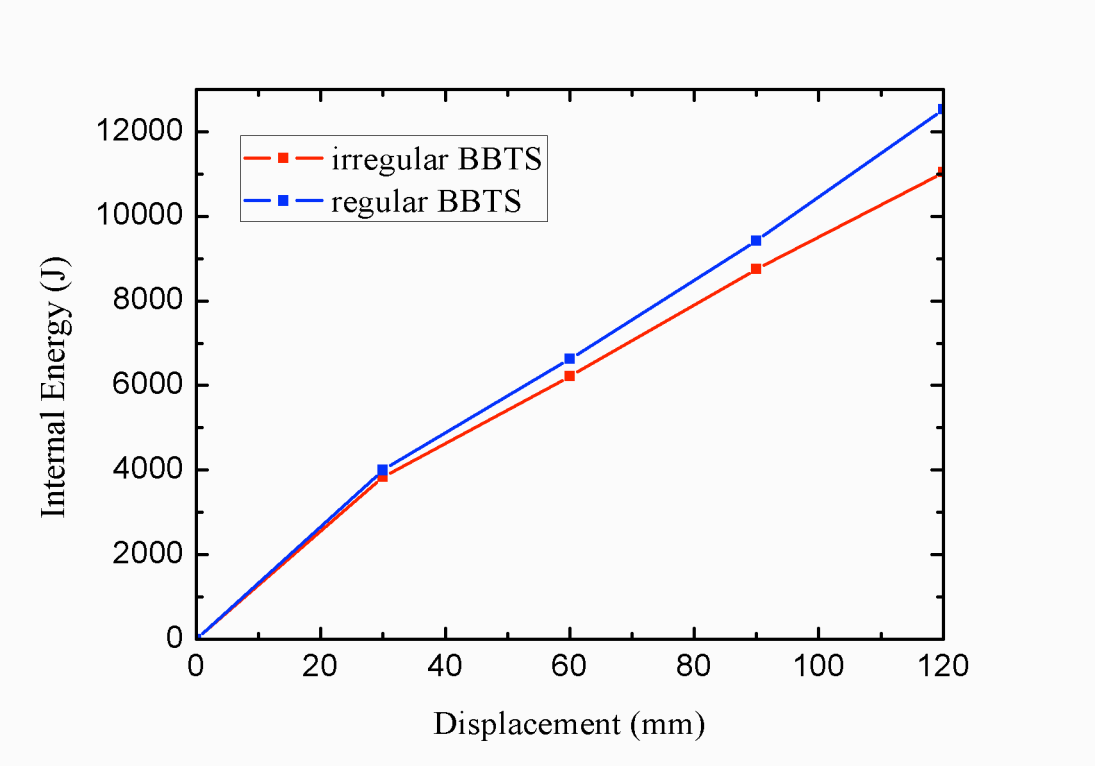

Fig.19. Absorbed energy-displacement curves of regular and irregular BBTSs.

Table 1

Mechanical properties of the aluminum alloy material for the tubes.

Density (kg/m^3)	Young's modulus (GPa)	Yield stress (MPa)	Ultimate stress (MPa)	Poisson's ratio
2700	68.2	162	192	0.3

Table 2

Design variables of different outer wall cases.

Case	1	2	3	4	5	6
t (mm)	0.8	1.2	1.6	2.0	2.4	2.8
d (mm)	49.52	32.34	23.56	18.13	14.37	11.58

List of figure captions

Fig.17. Crashworthiness criteria of BBTSs with different inside column diameter of 6 cases: (a) SEAs, (b) MIFs, and (c) CLEs.

Fig.18. Boundary and initial conditions of FE models of BBTS: (a) irregular BBTS, and (b) regular BBTS.

Fig.19. The absorbed energy versus displacement curves of regular BBTS and irregular BBTS.